applied sciences

MDPI

Article

Study on Microscopic Characteristics and Rock Mechanical Properties of Tight Sandstone after Acidification–Supercritical CO_2 Composite Action: Case Study from Xujiahe Formation, China

Yunfei Zhao [1,2], Gun Huang [1,2,*], Qinming Liang [1,2] and Qiang Chen [1,2]

1 State Key Laboratory of Coal Mine Disaster Dynamics and Control, Chongqing University, Chongqing 400044, China; 202120021017@stu.cqu.edu.cn (Y.Z.); 20182001006@cqu.edu.cn (Q.L.); 202320131112@stu.cqu.edu.cn (Q.C.)
2 School of Resources and Safety Engineering, Chongqing University, Chongqing 400044, China
* Correspondence: hg023@cqu.edu.cn

Abstract: Acidified CO_2 fracturing is a viable method for increasing production in deep, tight sandstone reservoirs. However, the potential mechanism of changes in pore structure and mechanical properties of sandstone under acidified CO_2 supercritical composite is not clear. Understanding this mechanism is important for the study of crack initiation and extension in tight sandstone reservoirs. This study utilizes sandstone samples from the Xujiahe Formation reservoir in Rongchang District as experimental specimens. The primary focus is to analyze the changes in pore structure and mechanical properties of these samples after acidification–supercritical CO_2 composite action. Nuclear magnetic resonance (NMR) and uniaxial compression tests are employed as the main investigative techniques. The results show that there was a physicochemical synergy between the acidification–supercritical CO_2 composite effect; the crack initial stress, damage stress, and peak stress of the sandstone after 16 MPa supercritical CO_2 acidification treatment were reduced by 20%, 49.5%, and 49.8%, respectively; the crack volumetric strain accelerated and the sandstone evolved from brittle to ductile damage; and the larger pore space and microcracks of the sandstone increased significantly after the treatment, which can be attributed to the gradual dissolution of intergranular cement leading to the formation of new pores connected to the existing pore network. The change mechanism of sandstone after acidification–supercritical CO_2 compound treatment is also proposed.

Keywords: acidification; supercritical CO_2; mechanical property; microscopic features; reservoir modification

check for updates

Citation: Zhao, Y.; Huang, G.; Liang, Q.; Chen, Q. Study on Microscopic Characteristics and Rock Mechanical Properties of Tight Sandstone after Acidification–Supercritical CO_2 Composite Action: Case Study from Xujiahe Formation, China. *Appl. Sci.* **2024**, *14*, 4108. https://doi.org/10.3390/app14104108

Academic Editor: Luca Fiori

Received: 11 April 2024
Revised: 4 May 2024
Accepted: 8 May 2024
Published: 12 May 2024

1. Introduction

Tight sandstone gas, as an unconventional natural gas resource, has garnered considerable attention due to its abundant reserves. In China, significant deposits of tight sandstone gas are mainly found in the Sichuan Basin, the Ordos Basin, and the Tarim Basin [1,2]. The unique geological conditions in these areas have resulted in tight gas reserves that are even more abundant than those of conventional natural gas [3–5]. Take the Shujiahe Formation reservoir in Rongchang District as an example. While tight sandstone gas reserves are substantial and hold great potential for development, the denseness of the formations typically leads to high fracture pressures, which present challenges for current wellhead pressure control equipment to effectively tap into these reservoirs [6,7]. As exploration and development of unconventional oil and gas resources reach greater depths, this issue becomes increasingly prominent [8,9]. Consequently, reducing the crack initiation pressure in reservoirs is one of the main factors to consider for large-scale exploitation of tight sandstone gas fields. Currently, supercritical CO_2 fracturing [10] is a promising waterless fracturing technique that holds potential for developing unconventional oil and gas reservoirs, as it can reduce water consumption, mitigate reservoir and environmental pollution, lower rock initial pressure, and also achieve partial carbon sequestration. Studies have demonstrated that acid treatment, while reducing the fracture pressure of reservoirs, can also enhance the physical properties of the reservoirs [11]

Zhao et al. [12] analyzed the effects of acid concentration, acid dosage, and acid reaction time on hydraulic fracture heterogeneity and fracture extension. The results show that the main factor affecting fracture extension was acid concentration followed by acid dosage, and the effect of acid reaction time was minimal. Li [13] studied the initiation and extension characteristics of fractures under different fracturing methods through physical and numerical simulations. They found that acid pressure effectively reduced the pressure of crack initiation and extension, and that the use of thickeners slowed the acid-rock reaction and increased the transmission distance of the acid [14]. Compared with acid pressure, the combined action of thickener and acid pressure made the crack initiation and extension more obvious, leading to more micro-cracks around the main crack. Gao et al. [15] used the discontinuous deformation analysis (DDA) method to study the effect of dissolution on the shear behavior of rock cracks. This research provides an effective tool for the micro-quantification of hydrochemical damage. Acid treatment destroys the rock's frame structure and intergranular cementation [16,17], changes the internal stress, and reduces the stress required for crack extension. This leads to the enhancement of subcritical crack extension and a reduction in rock strength [18,19]. Zhou et al. [20] analyzed the physical characteristics of loose sandstone reservoirs under lower supercritical CO_2 pressure and discovered that supercritical CO_2 under low pressure conditions reduced the permeability of sandstone reservoirs. Liang et al. [21] studied sandstone after soaking in supercritical CO_2 for different lengths of time, which had a significant weakening effect on the mechanical properties of the top sandstone.

Research indicates that pore structure plays a significant role in the dissolution of rock minerals and changes in porosity [22]. Changes in microstructure are strongly influenced by the distribution of minerals. In addition, the physical properties of the reservoir are determined by the pore structure and microcracks [23], which are abundant in loose sandstones, so it is necessary to study the pore structure and microstructure quantitatively. Nuclear magnetic resonance (NMR) technology, as a non-destructive testing method, is widely used in the study of pore structure characteristics in oil and gas reservoirs. By combining XRD and SEM scanning electron microscopy, a deeper understanding of the changes in the pore structure characteristics of tight sandstone under the composite action of acidification and supercritical CO_2 can be achieved by comparing untreated and singly treated sandstones. Following this, uniaxial compression tests were conducted on the rock samples to analyze the changes in their mechanical properties [24]. Previous studies have shown that both acid treatment and supercritical CO_2 soaking can alter the pore structure and mechanical properties of rocks. However, research on the evolution of sandstone pore structures under the composite action of acidification and supercritical CO_2 is limited. Therefore, this study employs NMR technology to investigate the evolution of sandstone porosity under different treatment conditions and to study its mechanical properties, providing a theoretical and experimental basis for reducing the initial stress of reservoir reconstruction in Rongchang District.

2. Materials and Equipment

2.1. Sample Preparation

In this study, sandstone cores from the Xujiehe Formation reservoir in Rongchang District, Chongqing, were used as experimental samples. The sampling depth was approximately 3100 m. The sampling location and reservoir geological section map are shown in Figures 1 and 2. Rongchang District, primarily located in the eastern Sichuan Basin and belonging to the eastern Sichuan high-steep fold belt, features reservoir sandstone lithology mainly composed of feldspar quartz sandstone and lithic quartz sandstone, followed by feldspathic lithic sandstone. Within the detrital grains, quartz content ranges from 65% to 90%, primarily consisting of monocrystalline quartz and metamorphic quartzite lithic fragments. Feldspar content varies between 2% and 21%, with plagioclase being the dominant type. Lithic fragments account for 4% to 24% of the composition, averaging 11.52%, and are mainly composed of sedimentary lithic fragments, followed by metamorphic and volcanic lithic fragments in decreasing abundance. Pore-filling materials exhibit a relatively high matrix content, averaging 3.67%. Cement content is comparatively low, with varying degrees of development observed in carbonate minerals (such as calcite), siliceous materials, and clay minerals. During the early stages of diagenesis, intergranular pores are filled with carbonate cements. Detrital grains commonly range from 0.25 to 0.5 mm in size, displaying moderate sorting, a grain-supported texture, and linear–concave–convex contacts [25].

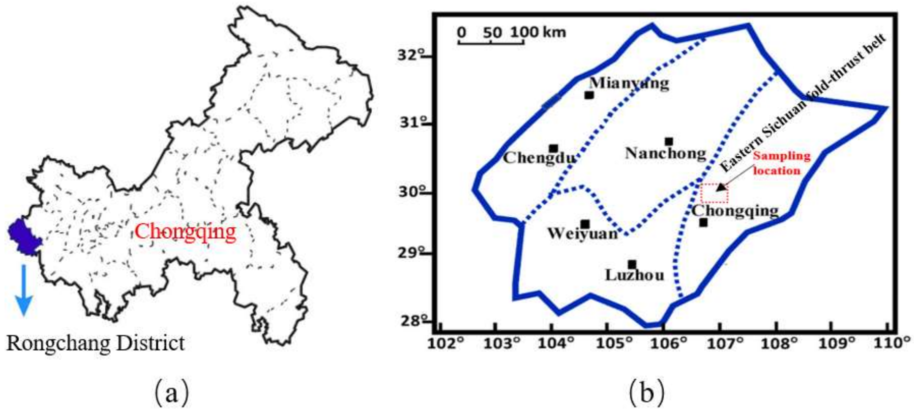

Figure 1. Sandstone core sampling locations. (**a**) Schematic map showing the location of the Rongchang basin in Chongqing. (**b**) Sampling location diagram.

Series	Formation	Symbol	Depth (m)
Cretaceous		K	1000
Upper Jurassic	Penglaizhen Suining	J_3p J_3sn	2000
Middle Jurassic	Shaximiao	J_2s	2700
L. Jurassic	Baitianba	J_1b	3000
Upper Triassic	Xujiahe	Xu5 or T_3x^5	
		Xu4 or T_3x^4	
		Xu3 or T_3x^3	
		Xu2 or T_3x^2	5000
		Xu1 or T_3x^1	

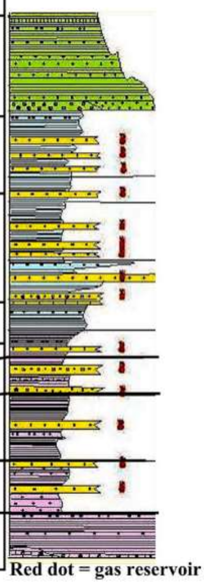

Figure 2. Reservoir geological section map. The yellow formations are gas-bearing sandstones.

In accordance with the standards recommended by the International Society for Rock Mechanics and Rock Engineering, the samples were processed with a height-to-diameter ratio of 2:1, with a diameter of 25 mm and a height of 50 mm. To ensure the accuracy of the tests, all samples were drilled from the same sandstone block; anomalous samples were eliminated using longitudinal wave velocity. The parallelism of the sample end surfaces was controlled to within 0.05 mm. Ultimately, 20 samples were selected and divided into 10 groups with 2 samples each.

The samples were first dried in a vacuum oven for 48 h at a temperature of 60 °C. After cooling to room temperature, they were subjected to different treatments: acid treatment (labeled sh-1, sh-2) with a mixture of 12% hydrochloric acid and 1% HF or 3% HF, supercritical CO_2 treatment (labeled co-1, co-2, co-3, co-4), acid–supercritical CO_2 composite treatment (labeled sc-1, sc-2, sc-3, sc-4), and untreated controls (y-1). The CO_2 soaking pressures were 10, 12, 14, and 16 MPa, respectively, with a temperature of 80 °C. According to the existing fracturing construction experience in the region, the acid used for treatment was a mixture of 12% hydrochloric acid and 2% HF with a concentration ratio of 6:1. Two samples were tested for each level of supercritical CO_2 soaking pressure, with control groups consisting of untreated, solely acid-treated, and supercritical CO_2-treated samples.

2.2. Experimental Equipment and Procedure

The High-Temperature and High-Pressure Sandstone Impregnation Device is a device independently developed by Chongqing University for supercritical CO_2 impregnation of sandstone. The equipment consists of a high-temperature control system, a high-temperature and high-pressure reaction kettle, pressure sensors, temperature sensors, a vacuum pump, and a high-precision plunger pump, among other components.

Uniaxial testing utilizes the MTS815 Rock Mechanics Testing System. The MTS815 is a hydraulic servo mechanical system produced by MTS Corporation in the United States primarily used for testing the mechanical properties and permeability of rocks, concrete, and coal bodies under complex stress conditions. The system has high precision and stable performance, and can perform high- and low-speed data collection. It employs control methods such as force, displacement, axial strain, and transverse strain, with a maximum axial loading capacity of 2800 kN and a maximum confining pressure of 80 MPa. The experimental steps are as follows:

After acid treatment, supercritical CO_2 treatment, and acid–supercritical CO_2 combined treatment, the samples were subjected to XRD (scanning angle of 0–90°) and NMR tests. First, the samples were immersed in distilled water to leach out the residual acid within the samples, followed by water saturation treatment at 5 MPa pressure for 12 h (Figure 3). NMR was used to test the saturated samples and analyze the effect of acid treatment on pore development. The NMR test parameters were set as follows: waiting time of 1.5 s, echo spacing of 0.2 ms, and echo number of 8000. Uniaxial compressive strength tests were conducted on the samples under different treatment conditions using an MTS815 testing machine. The samples were placed on the testing platform, and a small axial load was applied to ensure complete contact between the indenter and the sample. The loading rate of the uniaxial compression test was set to 0.1 mm/min, and circumferential extensometers were used to measure radial strain.

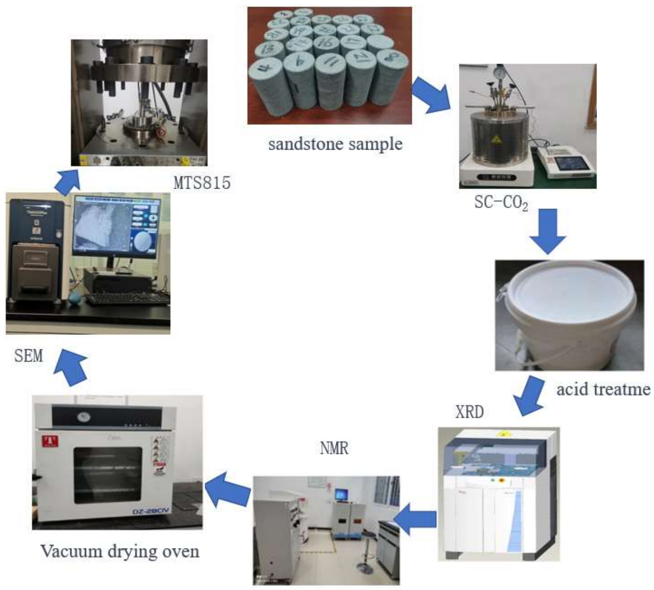

Figure 3. Experimental system procedure.

3. Results and Discussion

3.1. NMR Data Analysis

NMR technology is widely used in the characterization of rock pore structure by examining the variation in relaxation time of hydrogen fluid in different pores [26]. According to the pore division rules of the International Union of Pure and Applied Chemistry (IUPAC), pores with a relaxation time of between 0 and 10 ms are defined as micropores, those of between 10 and 100 ms are defined as mesopores, and those greater than 100 ms are defined as macropores. As shown in Figure 4, the T_2 spectra of the sandstone samples after different treatments are shown. By comparison, it can be seen that the pore size distribution curve of the untreated sandstone sample is not noticeably bimodal. The main peak is approximately at T_2 2.1 ms, which belongs to small pores and corresponds to a pore component of about 0.37%. The secondary peak is approximately at T_2 74 ms, which belongs to mesopores and corresponds to a pore component of about 0.145%. The T_2 spectra before treatment of the sandstone samples under different treatment conditions show no significant difference, mainly small and medium pores with a relatively continuous distribution, indicating that the sandstone is relatively tight.

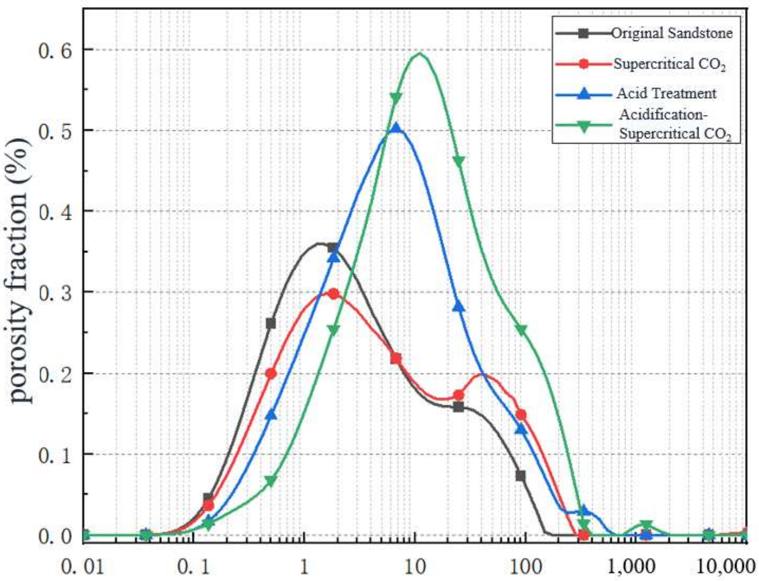

Figure 4. T_2 spectra of sandstone under different treatment conditions.

As shown in Figure 3, after treatment with 14 MPa CO_2, the peak position of the main peak of the sandstone sample begins to move to the right, and the porosity component rapidly decreases to 0.28, while the porosity component of the secondary peak is 0.20 and the secondary peak position is about 67 ms. This is because at a lower supercritical CO_2 soaking pressure, the ability of sandstone to combine water and CO_2 to form an acidic solution is low, leading to a low degree of acidification reaction, and due to adsorption expansion, the number of small pores in the sandstone decreases and large pores evolve into mesopores. As the soaking pressure gradually increases, the ability of sandstone to combine water and CO_2 to form an acidic solution gradually increases, and the degree of acidification reaction also intensifies, causing the sandstone mineral matrix to be partially dissolved and corroded and the ability of supercritical CO_2 to extract organic matter in the sandstone also to gradually increase. Although adsorption expansion still exists, at this time, the coupling of supercritical CO_2 extraction, acidification, and dissolution plays a dominant role, leading to an increase in the number of small and large pores in the sandstone.

After acid treatment, the T_2 of the sandstone evolves into a single peak shape. Compared to the original sandstone and supercritical CO_2 treatment, the main peak position rapidly moves in the direction of increase, and the main peak porosity component also increases significantly. After treatment with 1% HF and 12% HCl concentration soil acid (sh-1), the main peak position of the sandstone T_2 is 5.9 ms and the porosity component is 0.5%, and the soil acid solution has a stronger effect on the dissolution of filling minerals in sandstone pores.

Under the combined action of acidification and supercritical CO_2, the T_2 trend of the sandstone is similar to that of single acidification treatment. As shown in Figure 3, after the combined action of acidification and supercritical CO_2, the bimodal shape of the sandstone T_2 is not obvious, the main peak position rapidly moves in the direction of increase, and the main peak porosity component also increases significantly. After acidification–16 MPa CO_2 treatment, the position of the main peak of the sandstone sample and the porosity component increase to the maximum, which are 12.9 ms and 0.58%, respectively, while the porosity component of the secondary peak is 0.01 and the secondary peak position is about 890 ms. The amplitudes of the main peak and the secondary peak are both greater than those of single acidification or supercritical CO_2 treatment. This may be due to the synergistic effect of acidification and supercritical CO_2, which completely corrodes the filling minerals in the sandstone pores, and the number and radius of larger pore throats increase significantly.

Overall, the changes in the T_2 spectrum curves of the sandstone samples under different treatment conditions reflect the variation patterns of the internal pore structure. The increase in the area under the T_2 spectrum curve is most significant for the samples subjected to the combined effect of acidizing and supercritical CO_2 treatment. This indicates that the acidizing-supercritical CO_2 composite treatment dissolves a portion of the sandstone minerals, promoting the development of internal pores within the sandstone. Considering the heterogeneous distribution of internal pores in the sandstone, during the treatment process, the mud acid always preferentially enters the larger connected pores, dissolving the rock minerals on the pore walls and facilitating the continuous development of the pore structure. This process is invariably accompanied by the gradual disappearance and re-establishment of pore throat channels between pores of different sizes. These changes are primarily manifested in the different morphological characteristics of the T_2 spectrum curves of the samples and the transformation of the T_2 spectrum from a bimodal shape to a unimodal shape with only one prominent peak.

Porosity Change Analysis

The statistical results of the porosity of the sandstone samples under different treatment conditions are presented in Table 1 and Figure 5.

Table 1. Sandstone porosity under different treatment conditions.

Pretreatment Conditions	**Porosity/%**
Original sandstone	8.64
Sc CO_2	9.08
Acidification	11.28
Acidification-Sc CO_2	12.60

SC CO_2 here means supercritical CO_2 pretreatment.

Observations reveal that the permeability of the sandstone increases to varying degrees under the three treatment conditions compared to the original sandstone core. Specifically, the porosity of the sandstone increases from 8.64 to 9.08 after supercritical CO_2 treatment, with no significant change. Analysis suggests that the interactions between supercritical CO_2 and sandstone include gas pressure, adsorption expansion, acidification reaction, and organic matter extraction. After 16 MPa CO_2 treatment, although the gas pressure enhances the compression effect on the matrix, adsorption causes matrix expansion, the acidification reaction has a more pronounced effect on pore dissolution, and the unique ability of supercritical CO_2 to extract organic matter affects the organic matter in the sandstone sample, resulting in a combined influence of the four factors that increases the porosity by 0.44.

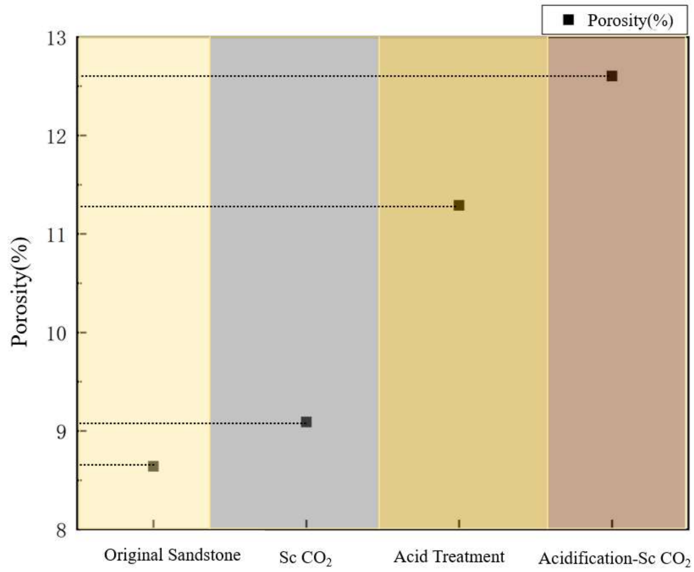

Figure 5. Sandstone porosity under different treatment conditions (including original sandstone, supercritical CO_2-treated sandstone, acid-treated sandstone, and acidification–supercritical CO_2 combined treated sandstone).

In contrast, the porosity of the sandstone after acidification treatment is 11.28, indicating that the acid has a more significant impact on the sandstone pore structure. Compared to single supercritical CO_2 treatment or acidification treatment, the porosity of the sandstone after acidification–supercritical CO_2 combined treatment reaches 12.6, which is higher than the sum of the porosity after supercritical CO_2 treatment and acidification treatment, which confirms that the acidification–supercritical CO_2 combined treatment is not simply additive but also exhibits synergistic effects. The reason is that the acidification treatment significantly increases the pore space of the sandstone, and the reactants and products of acid treatment provide an acidic environment for supercritical CO_2 to act on sandstone, promoting and catalyzing its effects.

3.2. Mechanical Property Analysis

3.2.1. Stress–Strain Analysis

Figure 6 presents the axial stress–strain curves of the sandstone samples under different treatment conditions. Supercritical CO_2 soaking and acid treatments significantly alter their mechanical strength and deformation characteristics. As observed from the graph, the axial stress–strain curves of all samples can be divided into four stages: initial pore compaction, elastic deformation, pre-peak yielding, and post-failure. The y-1 sample produces a noticeable sound upon failure, followed by a sharp drop in axial stress, indicating a clear brittle failure of the original sandstone sample. In contrast, the four groups of samples treated with the acid–supercritical CO_2 composite action (sc-1, sc-2, sc-3, sc-4) do not exhibit this distinct characteristic. Compared with the original sample, the peak strength and deformation of the sandstone decrease monotonically after being subjected to supercritical CO_2 soaking, acid treatment, and the acid–supercritical CO_2 composite treatment. The peak strength of the four groups of samples treated with supercritical CO_2 at pressures of 8 MPa to 16 MPa decrease by 1.2% to 32.7%; the two groups of samples subjected to acid treatment decrease by 20.3% to 26%, confirming that within a certain range, higher acid concentration and soaking pressure have a more pronounced effect on the strength of sandstone. However, the strength reduction in the four groups of sandstone samples treated with the acid–supercritical CO_2 composite is even more significant, with decreases ranging from 37.4% to 49.7% compared to the original sandstone sample. Compared to other samples, the axial stress–strain curves of sh-2, sc-1, sc-2, sc-3, and sc-4 exhibit a distinct pre-peak yielding stage, a level of deformation that falls within the category of brittle–ductile failure. This indicates that the sandstone exhibits certain ductile failure characteristics after complete acid reaction.

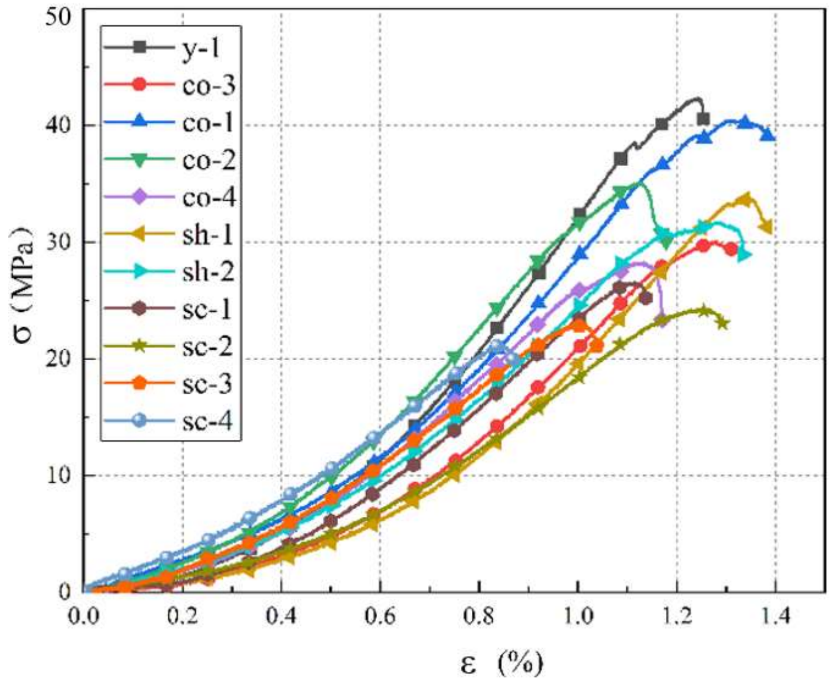

Figure 6. Uniaxial stress–strain curves of sandstone under different treatment conditions.

3.2.2. Determination and Analysis of Crack Initiation Stress and Damage Stress

In this study, the crack volume strain method is utilized to identify characteristic stresses in sandstone under different treatment conditions during uniaxial compression [27]. The rock undergoes volumetric, axial, and lateral strains, which are related as follows:

$$\varepsilon_{\mathrm{y}} + 2\varepsilon_{\mathrm{x}} = \varepsilon_v \tag{1}$$

where ε_{v} is the volumetric strain, ε_x is the lateral strain, and ε_y is the axial strain.

It is assumed that the volumetric strain of the rock ε_v consists of an elastic volumetric strain ε_{ev} and a crack volume strain $\varepsilon_{\mathrm{cv}}$, namely:

$$\varepsilon_{\mathrm{ev}} + \varepsilon_{\mathrm{cv}} = \varepsilon_v \tag{2}$$

The elastic volumetric strain ε_v is computed as:

$$\varepsilon_v = \varepsilon_1 + \varepsilon_2 + \varepsilon_3 \tag{3}$$

where ε_1 is the strain in the direction of the maximum principal stress σ_1, ε_2 is the strain in the direction of the intermediate principal stress σ_2, and ε_3 is the strain in the direction of the minimum principal stress σ_3.

Based on the generalized Hooke law, the formula for the elastic volumetric strain ε_{ev} is obtained as:

$$\varepsilon_{\mathrm{ev}} = \frac{1-2\mu}{E}(\sigma_1 + \sigma_2 + \sigma_3) \tag{4}$$

where μ is the Poisson ratio and E is the elastic modulus, determined from the elastic deformation stage.

For uniaxial compression, where $\sigma_2 = \sigma_3 = 0$, this further simplifies to:

$$\varepsilon_{\mathrm{ev}} = \frac{(1-2\mu)\sigma_1}{E} \tag{5}$$

From Equations (3) and (5), the crack-related crack volume strain ε_{cv} is derived:

$$\varepsilon_{\mathrm{cv}} = \varepsilon_v - \varepsilon_{\mathrm{ev}} = \varepsilon_1 + 2\varepsilon_2 - \frac{(1-2\mu)\sigma_1}{E} \quad (6)$$

The volumetric strain ε_v, elastic volumetric strain ε_{ev}, and cracking volumetric strain $\varepsilon_{\mathrm{cv}}$ are calculated by means of Equations (1), (2), (3), (4), (5), and (6), respectively, as illustrated in Figure 7, which results in the appearance of two peaks in the ε_{v} and $\varepsilon_{\mathrm{cv}}$ curves. The peak point is vertically upward according to the stress–strain curve, and points B and C are obtained. Point B is the crack initiation stress of the specimen σ_{ci}, while point C is the damage stress of the specimen σ_{cd}. Finally, point D, which is the peak stress σ_c, is obtained according to the peak point of the stress–strain curve graph.

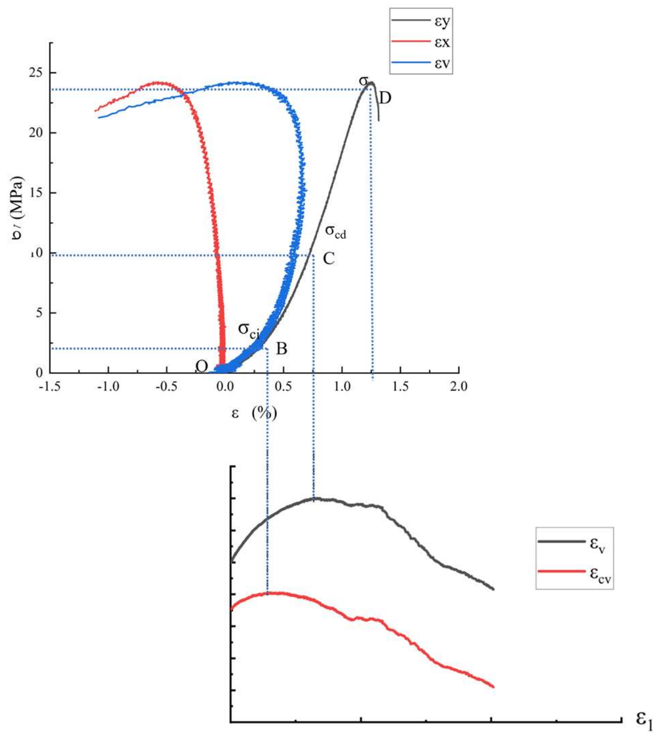

Figure 7. Determination of crack initiation stress in the damage stage of brittle rock.

Through the uniaxial compression experiments, the relationship between crack initiation stress and damage stress of the sandstone under acidification–supercritical CO_2 compounding is summarized, as shown in Figures 8 and 9.

The trend of damage stress of the specimens under three processing conditions is consistent with the trend of peak strength, both showing a monotonic decrease. Under supercritical CO_2 soaking conditions, as the soaking pressure increases, the initial stress of the sandstone gradually decreases, reaching a maximum value of 13 MPa at a soaking pressure of 8 MPa, which is close to the original sandstone initial stress of 14.3 MPa. When the soaking pressure is 16 MPa, the initial stress decreases to a minimum value of 11.4 MPa. Under the condition of sandstone acidization treatment, the initial stresses of sandstone soaked in low- and high-concentration hydrochloric acid are 12.5 MPa and 13.7 MPa, respectively, both lower than the original sandstone initial stress. It is evident that acidization treatment also has a significant impact on the initial stress of the sandstone, and within a certain concentration range, the higher the concentration of hydrochloric acid, the more significant the deterioration of the sandstone. Under the combined action of acidization and supercritical CO_2, the reduction in sandstone initial stress is more significant compared to solely acidization or supercritical CO_2 treatment, with a similar pattern to that of supercritical CO_2 soaking, averaging a 20% decrease and reaching maximum and minimum values of 12.5 MPa and 11.2 MPa at 8 MPa and 16 MPa, respectively. The reason for this phenomenon is that the combined effect of mud acid and supercritical CO_2 dissolves and extracts some sandstone minerals. According to the research of Zhang [28,29], the reservoir in this area is dominated by calcareous and siliceous cementation, and the reservoir pores are dominated by primary intergranular pores between clastic particles and dissolution pores produced by dissolution, which exacerbates the damage to the sandstone and reduces the initial stress of the sandstone.

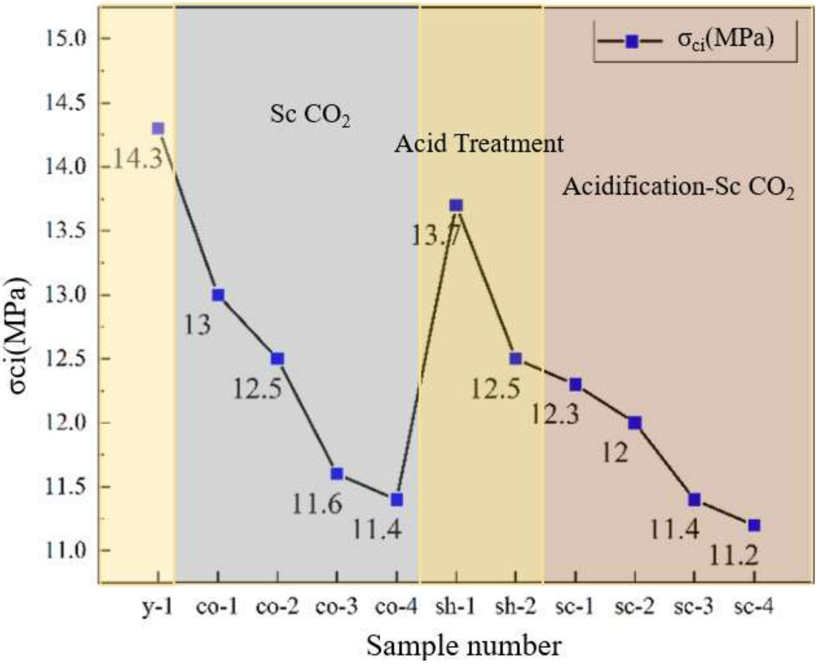

Figure 8. Stress curve of sandstone cracking under different pretreatment conditions.

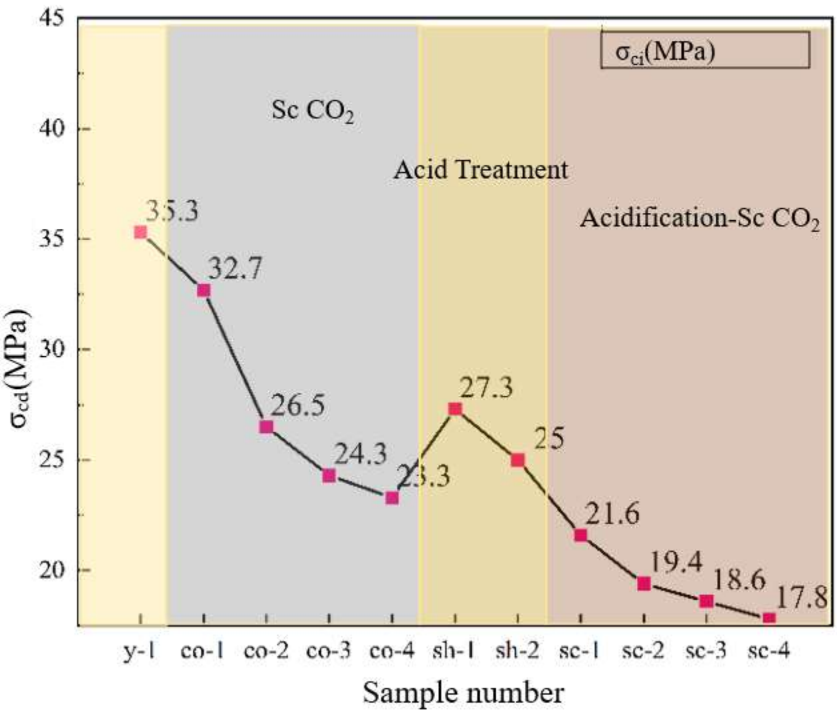

Figure 9. Damage stress curve of sandstone under different pretreatment conditions.

As shown in Figure 8, the trend of damage stress variation for specimens with different crack inclinations is similar to that of peak strength, both showing a monotonic decrease. Under supercritical CO_2 soaking conditions, as the soaking pressure increases, the damage stress of the sandstone gradually decreases, with a maximum value of 32.7 MPa at a soaking pressure of 8 MPa, which is close to the original sandstone damage stress of 35.3 MPa. When the soaking pressure reaches 16 MPa, the damage stress decreases to a minimum value of 23.3 MPa. Under the conditions of sandstone acidization treatment, the damage stresses of the sandstone soaked in low- and high-concentration hydrochloric acid are 27.3 MPa and 25 MPa, respectively, both of which are lower than the original sandstone damage stress. It is evident that acidization treatment also significantly impacts the damage stress of the sandstone, and within a certain concentration range, the higher the concentration of hydrochloric acid, the more significant the deterioration of the sandstone. Under the combined effect of acidization and supercritical CO_2, the reduction in sandstone damage stress is more significant compared to purely acidization or supercritical CO_2 treatment. The pattern of damage stress variation is similar to that of supercritical CO_2 soaking, with the maximum and minimum values being 12.5 MPa and 11.2 MPa at 8 MPa and 16 MPa, respectively, and a reduction range from 38.8% to 49.58%. The reason is that the combined action of hydrochloric acid and supercritical CO_2 dissolves part of the sandstone matrix, leaving large pores and making the pore network more complex. At the same time, the combined action of acidization and supercritical CO_2 leads to the expansion of existing cracks and the formation of new cracks. The chemical interaction between supercritical carbon dioxide and acidic substances can damage or destroy the mineral lattice structure in the sandstone, causing changes in its internal structure. Some minerals may be dissolved or partially dissolved, leading to damage to their lattice structures and thereby exacerbating the damage to the sandstone and affecting its overall stability and strength. This results in a reduction in damage stress to the sandstone.

3.2.3. Analysis of Sandstone Strain Variation

As shown in Figure 10, according to the definition, rock strain contraction is positive, and strain expansion is negative. It can be understood that the axial strain of the uniaxial compressed rock sample is always positive, while the lateral strain is always negative. In the failure stage, the lateral strain of the rock continuously increases. At this time, the volumetric strain of the rock sample changes from positive to negative, indicating a transition of the rock sample from compression to expansion.

The trends of the stress–strain curves of the sandstone under different treatment conditions are generally consistent, but there are certain differences between different pre-treatment conditions. Compared to the original sandstone, the pure acidization treatment and supercritical CO_2 treatment does not change the peak axial strain of the sandstone, while the axial deformation of the samples treated with both acidization and supercritical CO_2 decreases by 38.57%. The combined action of acidization and supercritical CO_2 leads to changes in the internal pore structure and physical properties of the samples, thereby altering their compressive performance and deformation characteristics. During the compression failure process of the sandstone samples under different treatment conditions, although the peaks are different, they all show a pattern of first increasing and then decreasing. The volumetric strain (εv) of the samples first contracts and becomes smaller and then gradually expands; at the same time, εv maintains positive values during the initial compaction stage, elastic deformation stage, stable crack expansion stage, and unstable crack expansion stage. As the volumetric strain reaches its peak, the peak point is the boundary where the sample transitions from compressive deformation to expansion and dilation. In the post-peak softening stage, as the expansion continues, εv will show negative values, resulting in volumetric expansion.

The evolution of crack volume strain during uniaxial compression of rock is related to axial strain, radial strain, the Poisson ratio during the elastic stage, and the elastic modulus. By substituting the experimental parameters into Equation (6), the evolution pattern of crack volume strain under different pretreatment conditions can be obtained, as shown in Figure 11.

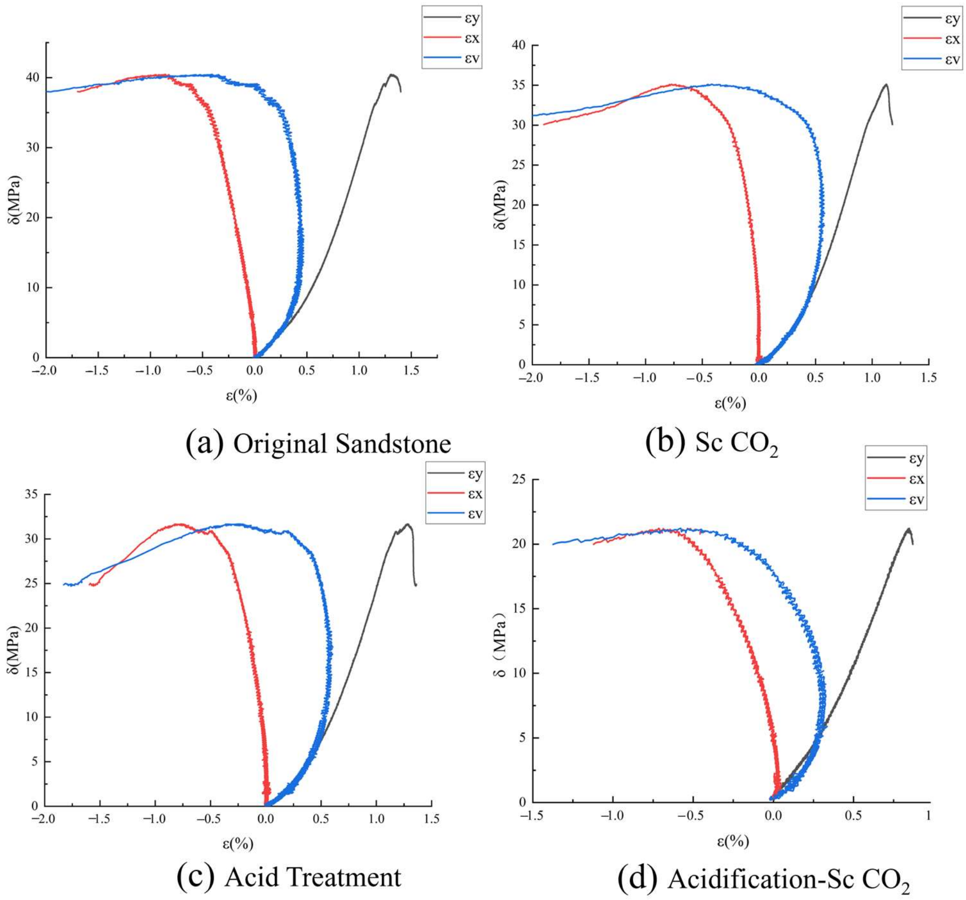

Figure 10. Stress–strain curves of sandstone under different treatment conditions.

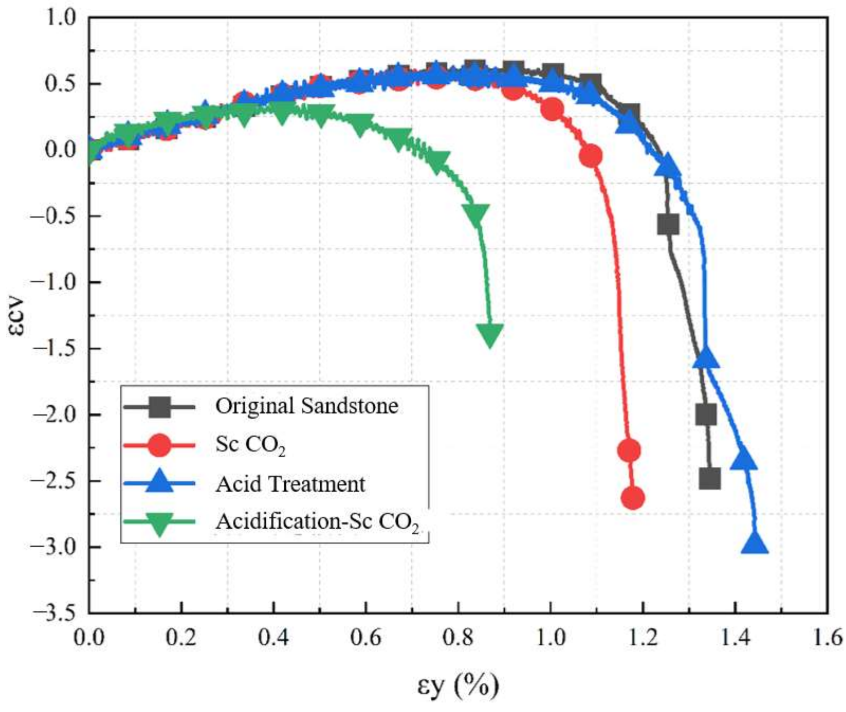

Figure 11. Characteristics of crack volume evolution in sandstone under different treatment conditions.

From Figures 3–10, it is evident that the combined action of acidization and supercritical CO_2 accelerates the rate of increase in crack volumetric strain in the sandstone, manifesting as a rapid expansion of internal crack volume in the sandstone. However, at the initial stage of loading, the crack volumetric strain of each group of rock samples changes from negative to nearly 0, indicating that the initial cracks inside the sandstone are compressed and closed during this phase. Additionally, it is found that, with the exception of the original sandstone samples, as the soaking pressure of supercritical CO_2 increases, the growth rates of crack volumetric strain in the sandstone increases to 3.26, 4.24, and 5.29, respectively, and the range of strain growth also gradually expands. This indicates that the action of acidization and supercritical CO_2 enhances the ductility of the rock samples, causing the overall deterioration of the samples, which leads to frequent interconnection of internal cracks and continuous aggravation of structural damage.

From the T_2 spectrum, it is known that the internal pores in the original sandstone are unevenly developed, with significant anisotropy. Under the influence of no pretreatment deterioration and axial load, the process of crack opening and closing alternates, and the crack volumetric strain fluctuates significantly, eventually increasing to 0.346. However, after treatment with acidization and supercritical CO_2, the crack volumetric strain in the sandstone exhibits stronger continuity and the curve is relatively smoother. At the same time, the original sandstone, under the action of axial load, experiences stress concentration at local defects, accelerating the destruction of the rock sample. Hence, the crack volumetric strain increases in speed and reaches its maximum in the later stages. However, for the acidization- and supercritical CO_2-treated samples, the overall deterioration reduces the prominence of local stress concentration, and the damage primarily progresses gradually.

3.3. Mechanism of Sandstone Changes after Acidification–Sc CO_2 Treatment

Rock is generally composed of matrix, detritus, and pores, exhibiting strong heterogeneity and anisotropy. The matrix grains, minerals, and cementing materials primarily determine the rock's strength, brittleness, and deformation characteristics, while pores and microcracks are the primary storage locations for water and hydrocarbon resources.

The XRD diffraction pattern of the sandstone before and after acidification–supercritical CO2 composite action is shown in Figure 12. According to the X-ray diffraction pattern, the mineral composition of tight sandstone is mainly quartz, feldspar, and chlorite. The diffraction peak intensity of quartz, chlorite, and feldspar in the sandstone minerals decreases to varying degrees after acidification–supercritical combined action. Table 2 shows the XRD (X-ray diffraction) test results, which are a comparison of the initial sample (y-1), the sample treated with acid for 24 h (sh-1), the sample treated with supercritical CO_2 (co-1), and the sample treated with acid–supercritical CO_2 (sc-1).

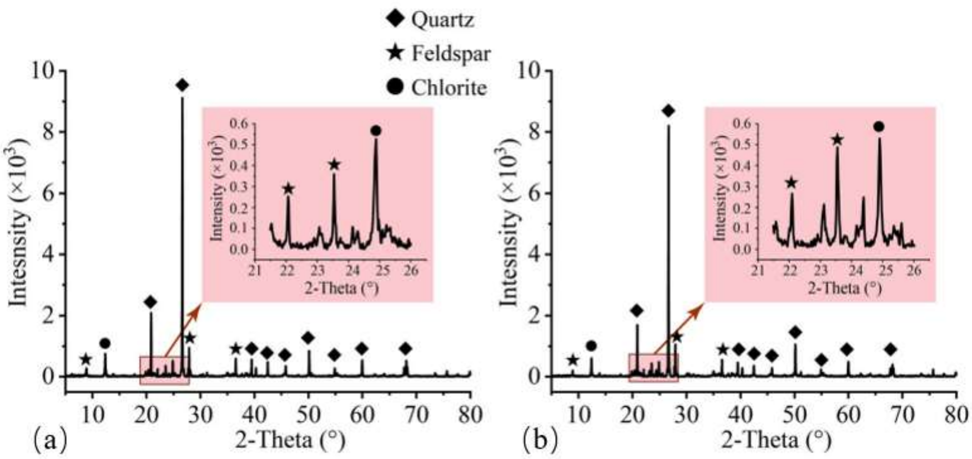

Figure 12. XRD diffraction patterns of y-1 (**a**) and SC-4 (**b**).

Table 2. Statistical results of XRD testing.

Pretreatment Conditions	Mineral Composition			
	Quartz (%)	**Feldspar (%)**	**Clay Minerals (%)**	**Magnesite (%)**
Original sandstone	42.1	2.4	51.6	3.9
Sc CO_2	45.7	2.3	48.1	3.9
Acid treatment	54.8	1.3	41.2	2.7
Acidification–Sc CO_2	62.5	0.7	34.2	2.6

XRD analysis indicates that the mineral composition of the compact sandstone is primarily quartz, feldspar, and clay minerals. After single supercritical CO_2 treatment, only the quartz content is significantly reduced, while after acid–supercritical CO_2 combined treatment, the content of quartz, feldspar, and green clay minerals in the sandstone mineral significantly decreases. This observation suggests that certain sandstone minerals dissolve due to the acid–supercritical CO_2 combined action. SEM images (Figure 13) after acid treatment show that acid dissolution destroys the bonding between the matrix grains, forming numerous microcracks and further increasing the width of initial microcracks. This ultimately results in the weakening of the sandstone's mechanical properties.

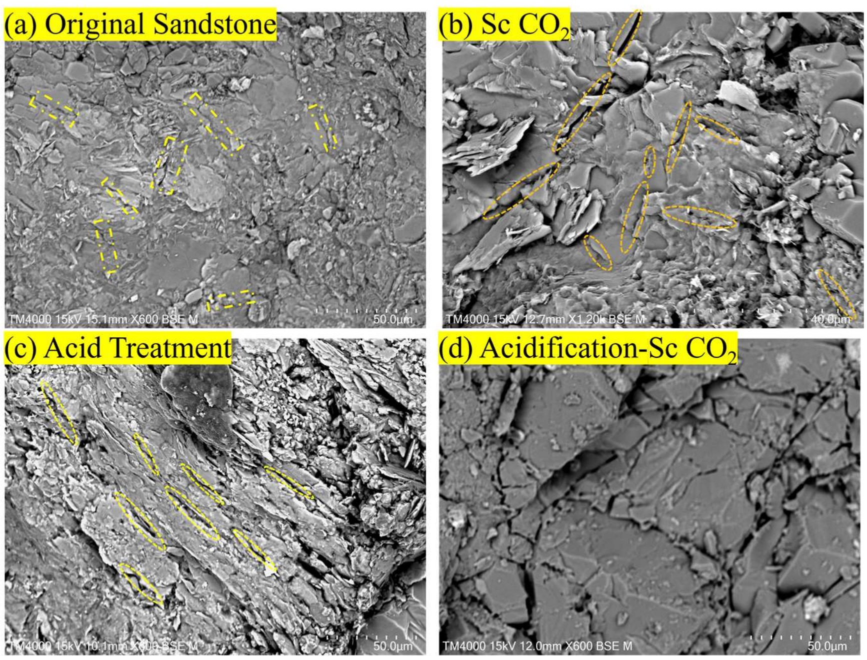

Figure 13. Images magnified 600× of local microcracks in sandstone under different treatment conditions.

Figures 13 and 14 present enlarged images of the surface morphology of the sandstone samples under different treatment conditions.

Observing the local crack on the surface of the untreated sandstone sample under 600× magnification (a), it can be seen that the sample surface is generally intact and dense, with barely visible microcracks between the matrix. Quartz, green clay minerals, and other minerals are scattered on the sample surface, and some mineral particles have rigid grain edge pores, with a clear boundary between mineral particles and a tight cementing structure. After treatment at 16 MPa CO_2, the mineral bonding water is extracted and captured by supercritical CO_2, generating HCO_3-, which undergoes secondary ionization to produce H^+ and carbonate salts, resulting in full dissolution. The sample surface morphology is partially destroyed and can be seen by the naked eye, with a significant increase in the number of pores and microcracks, even forming collapse pores. Mineral particle edges show clear boundaries, indicating that the tight cementing structure between mineral particles has been partially destroyed, and under fluid action, it is possible to observe mineral particles being peeled off. After acid treatment, the sandstone sample surface becomes rough and changes from gray to light yellow (Figure 15). Under SEM observation, it is found that surface minerals are dissolved, generating numerous irregular intergranular corrosion pores, and the morphology is significantly destroyed. The number of pores and microcracks increases significantly, and acid treatment further enlarges the initial microcrack width, providing a favorable space for subsequent supercritical CO_2 action on the sandstone.

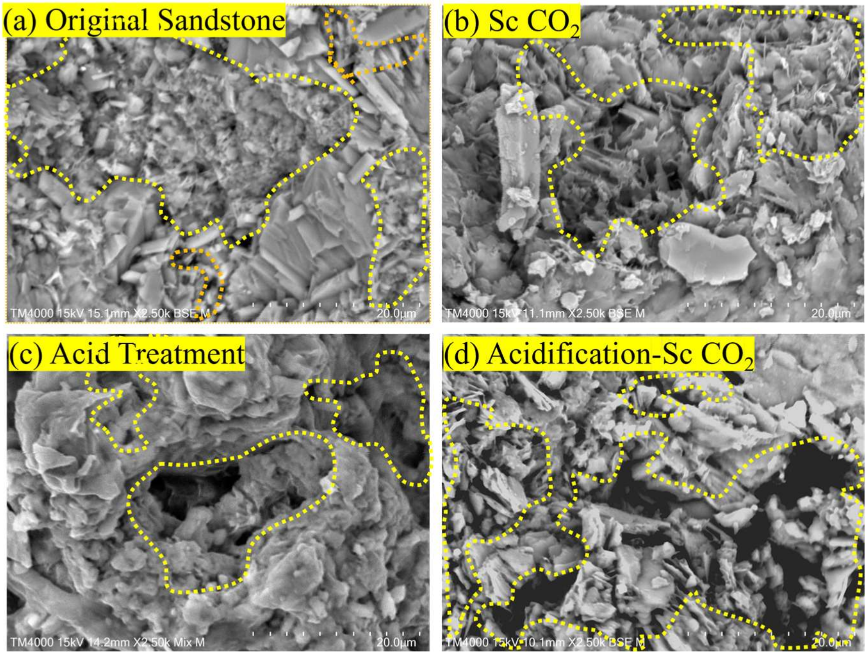

Figure 14. Images magnified 2500× of local sandstone morphology under treatment conditions.

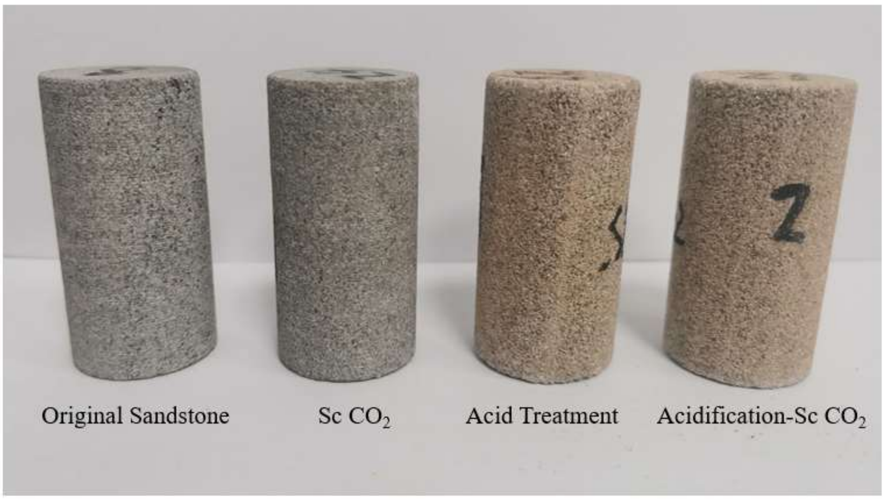

Figure 15. Changes in sandstone surface under different treatment conditions.

Compared with untreated sandstone, single acidization, or supercritical CO_2 treatment, acidization–supercritical CO_2 combined processing leads to more significant degradation of the sandstone. The pre-treatment of acid significantly increases the porosity of the sandstone, thereby greatly increasing the reaction volume between supercritical CO_2 and the sandstone. Residual acidic reaction materials and reaction products alter the pH environment of the supercritical CO_2 and sandstone minerals, causing the acid treatment to interact with the supercritical CO_2 and sandstone. Under scanning electron microscopy, the sandstone morphology changes drastically after acidization–supercritical CO_2 combined action: The sample surface becomes rough, similar to single acid treatment, and the color changes from gray to light yellow. The clay minerals in the sandstone are severely dissolved by acid, the feldspar reacts with hydrofluoric acid to be significantly dissolved, and the quartz also partially reacts with hydrofluoric acid. The carbonate in the sandstone pores, the green clay minerals at the edge of the pores, and the illite filling are dissolved or only leave traces by the acid solution, supercritical CO_2, and water-generated H^+. The mineral matrix on the sample surface is dissolved, generating numerous irregular intergranular corrosion pores, and the morphology is severely destroyed. The number of pores and microcracks is significantly increased compared to single acidized sandstone, and the initial microcrack width and length are also greatly increased, with the area of collapse voids further expanding. At the same time, the boundaries of mineral particles become apparent, indicating that the tight cementing structure between mineral particles is severely destroyed. This shows that sandstone acid treatment promotes and catalyzes the reaction between sandstone and supercritical CO_2.

4. Conclusions

This paper mainly investigates the changes in pore structure and mechanical properties of sandstone reservoirs after acidification–supercritical CO_2 composite treatment. The main conclusions are:

(1) The continuity of the T_2 spectral curve of the sandstone samples is not obvious. The acidification–supercritical CO_2 composite treatment results in the dissolution of a large number of minerals after the composite treatment, which makes the pore size distribution more uniform, and the T_2 spectral curve is trapezoidal, which is more favorable for the development of pores into macropores (T_2 335 ms) and mesopores (T_2 6.85 ms).

(2) The acidification–supercritical CO_2 composite treatment has a significant effect on the pore size distribution and permeability of the sandstone. Compared with the sandstone under untreated or single treatment conditions, the chlorite, feldspar, and carbonate contents of the sandstone after the composite treatment are significantly reduced; the morphology of the sandstone is dramatically changed, and the number of initial microcracks is also dramatically increased after the acidification–supercritical CO_2 composite action.

(3) After the acidization–supercritical CO_2 composite treatment, the peak strength, initial stress, and damage stress of the sandstone decreases by 49.7%, 20%, and 49.5%, respectively. The composite treatment accelerates the growth rate of crack volume strain in the sandstone; enhances the ductility of the samples; causes overall deterioration of the samples, leading to frequent intercrossing of internal cracks; and exacerbates structural damage.

(4) Acid pretreatment greatly increases the pore volume of the sandstone and then greatly increases the volume of supercritical CO_2 and sandstone, while the residual acidic reactants and reaction products change the PH environment of supercritical CO_2 and sandstone mineral solubility, so there is a physicochemical effect of acid treatment on the reaction between supercritical CO_2 and sandstone.

Author Contributions: Conceptualization, Y.Z. and G.H.; methodology, Q.L.; validation, Q.C. and Y.Z.; formal analysis, Q.C.; writing—original draft preparation, Y.Z. and G.H.; writing—review and editing, Y.Z. All authors have read and agreed to the published version of the manuscript.

Funding: This work is financially supported by grants from the National Science Foundation of China (Grant No. 51674049).

Institutional Review Board Statement: Not applicable.

Informed Consent Statement: Informed consent was obtained from all subjects involved in the study.

Data Availability Statement: The raw data supporting the conclusions of this article will be made available by the authors on request.

Acknowledgments: The authors are grateful for the support.

Conflicts of Interest: The authors declare no conflict of interest.

References

1. Li, S.; Qiao, D. Current situation of tight sand gas in China. In Proceedings of the International Conference on Energy, Environment and Sustainable Development (ICEESD 2011), Shanghai Univ Elect Power, Shanghai, China, 21–23 October 2012; Shanghai Univ Elect Power: Shanghai, China, 2011; p. 85.
2. Zou, C.; Tao, S.; Han, W.; Zhao, Z.; Ma, W.; Li, C.; Bai, B.; Gao, X. Geological and Geochemical Characteristics and Exploration Prospect of Coal-Derived Tight Sandstone Gas in China: Case Study of the Ordos, Sichuan, and Tarim Basins. *Acta Geol. Sin.-Engl. Ed.* **2018**, *92*, 1609–1626. [CrossRef]
3. Dai, J.; Ni, Y.; Wu, X. Tight gas in China and its significance in exploration and exploitation. *Pet. Explor. Dev.* **2012**, *39*, 277–284. [CrossRef]
4. Ma, X.; Jia, A.; Tan, J.; He, D. Tight sand gas development technology and practices in China. *Pet. Explor. Dev.* **2012**, *39*, 611–618. [CrossRef]
5. Chen, Y.; Yang, J.; Talha, M.; Xia, Y.; Tang, M.; Xie, R. Sequence Stratigraphy of the Jurassic Strata and Occurrences of Potential Sandstone Reservoirs in the ST Gas Field, Northern West Siberia Basin. *Appl. Sci.* **2023**, *13*, 12096. [CrossRef]
6. Li, N.; Chen, F.; Yu, J.; Han, P.; Kang, J. Pre-acid system for improving the hydraulic fracturing effect in low-permeability tight gas reservoir. *J. Pet. Explor. Prod. Technol.* **2021**, *11*, 1761–1780. [CrossRef]
7. Tan, P.; Jin, Y.; Hou, B.; Zheng, X.; Guo, X.; Gao, J. Experiments and analysis on hydraulic sand fracturing by an improved true tri-axial cell. *J. Pet. Sci. Eng.* **2017**, *158*, 766–774. [CrossRef]
8. Guo, C.; Xu, J.; Wei, M.; Jiang, R. Experimental study and numerical simulation of hydraulic fracturing tight sandstone reservoirs. *Fuel* **2015**, *159*, 334–344. [CrossRef]
9. Zou, C.; Zhu, R.; Liu, K.; Su, L.; Bai, B.; Zhang, X.; Yuan, X.; Wang, J. Tight gas sandstone reservoirs in China: Characteristics and recognition criteria. *J. Pet. Sci. Eng.* **2012**, *88*, 82–91. [CrossRef]
10. Hu, Y.; Liu, Y.; Cai, C.; Kang, Y.; Wang, X.; Huang, M.; Chen, F. Fracture Initiation of an Inhomogeneous Shale Rock under a Pressurized Supercritical CO_2 Jet. *Appl. Sci.* **2017**, *7*, 1093. [CrossRef]
11. Hou, B.; Zhang, R.; Chen, M.; Kao, J.; Liu, X. Investigation on acid fracturing treatment in limestone formation based on true tri-axial experiment. *Fuel* **2019**, *235*, 473–484. [CrossRef]
12. Zhao, H.; Xiong, Y.; Zhen, H.; Liu, C.; Li, X. Experimental investigation on the fracture propagation of three-stage acid fracturing of tight sandstone gas reservoir. *J. Pet. Sci. Eng.* **2022**, *211*, 110143. [CrossRef]
13. Li, H.; Shi, Y. Triaxial experimental investigation into the characteristics of acid-etched fractures and acid fracturing. *J. Pet. Sci. Eng.* **2021**, *202*, 108431. [CrossRef]
14. Wang, W.; Liu, T.G.; Shao, J.F. Effects of Acid Solution on the Mechanical Behavior of Sandstone. *J. Mater. Civ. Eng.* **2016**, *28*, 04015089. [CrossRef]
15. Gao, J.; Chen, G.; Mitani, Y.; Gong, S.; Feng, C. Study on the effect of hydro-chemical dissolution on shear properties of rock fractures using the improved discontinuous deformation analysis. *Int. J. Numer. Anal. Methods Geomech.* **2023**, *47*, 1457–1480. [CrossRef]
16. Luo, T.; Fan, G.; Guo, B.; Zhang, S. Experimental study on the influence of hydro-chemical erosion on morphology parameters and shear properties of limestone fractures. *Acta Geotech.* **2021**, *16*, 3867–3880. [CrossRef]
17. Zhang, H.; Zhong, Y.; Zhang, J.; Zhang, Y.; Kuang, J.; Yang, B. Experimental research on deterioration of mechanical properties of carbonate rocks under acidified conditions. *J. Pet. Sci. Eng.* **2020**, *185*, 106612. [CrossRef]
18. Grgic, D.; Giraud, A. The influence of different fluids on the static fatigue of a porous rock: Poro-mechanical coupling versus chemical effects. *Mech. Mater.* **2014**, *71*, 34–51. [CrossRef]
19. Martin, R.J. Time-Dependent Crack Growth in Quartz and Its Application to Creep of Rocks. *J. Geophys. Res.* **1972**, *77*, 1406–1419. [CrossRef]
20. Linsong, Z.; Jianfen, D.; Ping, G.; Zhouhua, W. Influence of Supercritical CO_2 on the Physical Property of Unconsolidated Sandstone Reservoir. *Oilfield Chem.* **2015**, *32*, 217–222.
21. Weiguo, L.; Wei, H.; Jiwei, Y. Weakening and fracturing mechanism of mechanical properties of coal and rock caused by supercritical CO_2. *J. China Coal Soc.* **2022**, *47*, 2557–2568.
22. Quanzhong, L.; Haiyang, H.; Xiaofeng, J. Research on differences in pore structures of coal, shale and sandstone and their effects on methane adsorption. *Coal Sci. Technol.* **2022**, *50*, 157–163.
23. Mahmoud, H. Automatic characterization and quantitative analysis of seismic facies in naturally fractured reservoir: Case study of Amguid Messaoud field, Algeria. *Min. Miner. Depos.* **2023**, *17*, 42–48. [CrossRef]
24. Ping, Q.; Li, X. Analysis of the Fracture Characteristics and Crack Propagation Mechanism of Fractured Sandstone under Dynamic Loading. *Appl. Sci.* **2024**, *14*, 2042. [CrossRef]
25. Liu, Y.; Xie, X.; Wang, Z.; Tan, J.; Zhao, Y. Biocomposition characteristics and potential evaluation of hydrocarbon generation in the Xujiahe Formation source rocks in the Sichuan Basin. *Nat. Gas Geosci.* **2024**, 1–17. Available online: https://www.cnki.com.cn/Article/CJFDTotal-TDKX20240305001.htm (accessed on 10 April 2024).

26. Geng, B.; He, X.; Yan, J.; Zhang, F.; Cui, Y.; Gu, J.; Li, Z.; Wen, D. NMR Based Low Permeability Sandstone Storage Layer Pore Structure Quantification Inversion Method, Involves Forming Wellbore Profile with Sand Rock Storage Layer along Reverse Inversion Direction. CN104819923-B, 15 May 2015.
27. Du, Y.; Li, T.; Wang, B.; Zhang, S.; Li, H.; Zhang, H.; Zhu, Q. Experimental study on mechanical characteristics and permeability evolution during the coupled hydromechanical failure of sandstone containing a filled fissure. *Acta Geotech.* **2023**, *18*, 4055–4075. [CrossRef]
28. Zhang, L.; Wang, W.; Shu, Z. Distribution and genesis of calcite-replaced and calcite-cemented tight reservoirs in Xujiahe Formation, Yuanba area, Northeast Sichuan. *Acta Pet. Sin.* **2019**, *40*, 692–705.
29. Zhou, Z. Reservoir Characteristics and Factors Controlling the Physical Properties of the Sandstone in the Forth Member of Xujiahe Formation in the Bazhong Area, Northeastern Sichuan Basin. Master Thesis, China University of Petroleum, Beijing, China, 2020.